ECS Transactions, 28 (23) 39-46 (2010)
10.1149/1.3502335 ©The Electrochemical Society

Improved Synthesis Method for a Cyanamide Derived Non-Precious ORR Catalyst for PEFCs

Ryan S. Hsu, and Zhongwei Chen*

Department of Chemical Engineering, Waterloo Institute of Nanotechnology, Waterloo Institute of Sustainable Energy, University of Waterloo, Waterloo, ON, N2L 3G1, Canada, zhwchen@uwaterloo.ca

Non-noble catalysts synthesized using an iron salt, cyanamide and Ketjen Black EC-600JD were developed as ORR active Fe-N/C materials for PEFC applications. The resulting initial Fe-cyan-KJ600 catalyst demonstrated poor ORR performance, however, through the addition of NH_3 during the pyrolysis treatment, and by modifications of the synthesis procedure to include a second coating and pyrolysis stage, the ORR performance increased drastically. The present study utilizes X-ray diffraction, scanning electron microscopy, nitrogen adsorption/desorption, and electrochemical analysis in characterizing the synthesized samples to determine the morphological and electrochemical effects of the aforementioned treatment steps.

Introduction

Polymer electrolyte membrane fuel cells (PEFC) have long been thought of as promising, clean, alternative energy electrochemical devices. Fuels such as H_2 or methanol are easily generated from a variety of sources, and when utilized with PEFCs can produce a device which generates low to no emissions. Despite these advantages, fuel cell technologies have failed to achieve mass commercialization mainly due to low operational lifetimes and high costs of materials. In particular, the membrane and the catalyst layer challenge the efforts made to reduce material costs. Scarce and expensive platinum currently remains the dominant material used to catalyze fuel cell reactions (1-3). In order to pursue the mass commercialization of fuel cells, two proposed methods have been sought: 1. Increase the utilization of platinum to lower the loading required and 2. eliminate the platinum metal completely through its replacement with a non-precious active material. The latter method has been suggested as the long term solution due to the increasing cost of platinum (4).

In recent literature, Dodelet's group reported a high ORR activity Fe-N/C catalyst with activity equivalent to that of platinum (5). In the study, they claim that the high activity was achieved through a high active site density on the carbon through the use of a porous carbon support. The formation of these active sites was believed to be assisted by the micropores of the carbon support which hosted many active sites.

From this research, several groups have developed this idea by using porous carbons to help increase the active site density of these types of electrocatalysts. Popov's group utilized a hard silica template to create a highly ordered nitrogen doped porous carbon electrocatalyst exhibiting high graphitization and surface area upwards of 1000 m^2/g (6). They were able to attribute their high ORR activity to high nitrogen content in the form

of quaternary and pyridinic type nitrogen which has been proposed to be the site for oxygen reduction. Pyridinic nitrogen forms on the graphitic edge of carbon which shows faster electrochemical kinetics compared to those on the basal plane. Various works experiment with different nitrogen precursors including, but not limited to polyacrylonitrile (6, 7), ethylenediamine (8, 9), polyaniline (10, 11), and ammonia (5, 7, 12, 13). Zelenay's group proposed cyanamide as a high nitrogen content precursor capable of forming pyridinic type nitrogen when pyrolyzed (14, 15).

In this present work, cyanamide (cyan) and Ketjen Black EC-600JD (KJ600) are utilized as an intrinsically high nitrogen content precursor and a commercial porous carbon support respectively. Modification of the synthesis procedure is intended to (a) develop a nitrogen-rich non-precious catalyst, (b) determine the effect of ammonia gas as an additional nitrogen precursor, and (c) attempt to increase the number of active sites on the catalyst surface by performing a second pyrolysis step. The novelty of this work stems from the combination of these treatments in order to optimize the activity of this catalyst with the addition of the alternate stages. Catalyst samples are physically examined by scanning electron microscopy (SEM), nitrogen adsorption/desorption, and X-ray diffraction (XRD) analyses. Rotating disc electrode (RDE) voltammetry is conducted for electrochemical measurements to evaluate the catalyst performance under acidic conditions.

Experimental

Functionalization of Carbon Black

Ketjen Black EC-600JD was functionalized prior to use by first treating the carbon black in HCl at room temperature, followed by a wash with de-ionized water. The product was fully dried in an oven overnight. Acid treatment of the product was done with HNO_3 at for 8 hours. The product was carefully filtered, and washed with de-ionized water before drying the functionalized carbon support at 80^{o}C overnight.

Synthesis of Fe-Cyan-KJ600 Electrocatalyst

Functionalized carbon was dissolved in HPLC grade ethanol and sonicated. Iron salt was completely dissolved in HPLC grade ethanol and mechanically stirred for 1 hour. Cyanamide was dissolved into ethanol and added drop-wise to the iron mixture under mixing conditions. This solution was kept stirring for 30 minutes before adding the mixture of carbon black together with the iron-cyanamide mixture. Using an oil bath and condenser tube, the solution was refluxed at 80^{o}C. The mixture was transferred to a beaker and the ethanol was allowed to evaporate under the same heating and mixing conditions. The solid precipitate collected was then allowed to dry in an oven at 60^{o}C overnight. The precipitated solid was pyrolyzed in a chemical vapour deposition furnace using N_2 or NH_3 as carrier gases resulting in catalyst samples Fe-cyan-KJ600-1 and Fe-cyan-KJ600-2 respectively. Finally, an acid leaching treatment was carried out using H_2SO_4 to remove any surface metals.

One sample (Fe-cyan-KJ600-3) underwent a re-pyrolysis to examine the effect of another pyrolysis stage on the performance of the cyanamide based catalyst. To go about the re-pyrolysis, the sample after acid leaching was ball-milled. The resulting sample was

then re-coated with iron and cyanamide as described previously at half loading. Pyrolysis and acid treatment was carried out as described above.

Disc Electrode Preparation

Electrochemical activity was measured through the use of rotating disc electrode experiments in a three-electrode half cell setup. A platinum wire was used as the counter electrode and an Ag/AgCl electrode was utilized as reference. All potentials were converted to the reversible hydrogen electrode (RHE) scale. Catalyst inks were made using HPLC grade ethanol with catalyst samples and sonicated until the catalyst was uniformly dispersed in the ink. Nafion was added on top of the electrocatalyst as a binding agent prior to conducting the experiments. Electrochemical measurements were obtained using a PINE AFCBP1 bipotentiostat in the range of 0.05-1.0V vs. RHE at 10mV/s in 0.1M $HClO_4$ while saturating the electrolyte with oxygen. The background current was removed by performing cyclic voltammetry experiments with the same conditions while bubbling N_2 gas in the electrolyte.

Physical Characterizations

All samples were analyzed by X-ray diffraction, scanning electron microscopy, and nitrogen adsorption/desorption analysis. XRD analysis was done with an Inel XRG 3000 diffractometer using a CuKα source. A broad range scan of the 2θ range from 0.288 to 113^o was captured for about 10 minutes per sample. A LEO FESEM 1530 was used to take SEM images at 100k times magnification at 20kV. XPS was carried out using a Thermal Scientific K-Alpha XPS spectrometer at 150eV to investigate the relative content of different elements and the relative content of different types of nitrogen. Brunauer, Emmett and Teller (BET) surface areas and pore size distributions were obtained through N_2 adsorption/desorption isotherms using an Autosorb 1 from Quantachrome Instruments. Prior to N_2 adsorption/desorption, samples were subject to an outgassing pretreatment by heating the sample at 100^{o}C in a vacuum overnight.

Results and Discussion

SEM analysis was carried out at various stages within the synthesis procedure and is shown in Figure 1. The micrographs show significant morphological changes of the catalyst at 100k times magnification. Figure 1a is an SEM image of functionalized Ketjen Black EC-600JD prior to use in the catalyst synthesis. Particles show uniform size distribution and no agglomeration. Although the pore channels cannot be seen from the micrograph, Ketjen Black EC-600JD is a high surface area carbon with significant pore volume - as later confirmed by nitrogen adsorption/desorption analysis. Figure 1b shows the Ketjen Black EC-600JD after the surface and pores have been coated with cyanamide and the iron precursor. This coating on the functionalized Ketjen Black EC-600JD can be observed from the SEM image as it is apparent that the average particle diameter has increased. The iron-cyanamide coating also induces agglomeration to occur between the Ketjen Black EC-600JD particles further decreasing specific surface area and causing blockage of the carbon pores. It can be seen in Figure 1c where catalyst sample (Fe-cyanamide-KJ600-2) has been pyrolyzed with ammonia and acid leached, that the iron-cyanamide coating seen in Figure 1b has been reduced and the particles are similar in shape and size distribution to the functionalized Ketjen Black EC-600JD. Smaller

particles are vital for increased surface area, increased access to pore channels, as well as, increased edge plane exposure of carbon to form higher pyridinic nitrogen within the catalyst. It is hypothesized that after pyrolysis with ammonia, the iron-cyanamide coating is effectively etched away leaving behind these nitrogen functionalities and Fe-N complexes believed to be the active sites. Figure 1d reveals the morphology of the Fe-cyan-KJ600-3 catalyst showing a drastic increase in particle size and severe agglomeration of the carbon black particles.

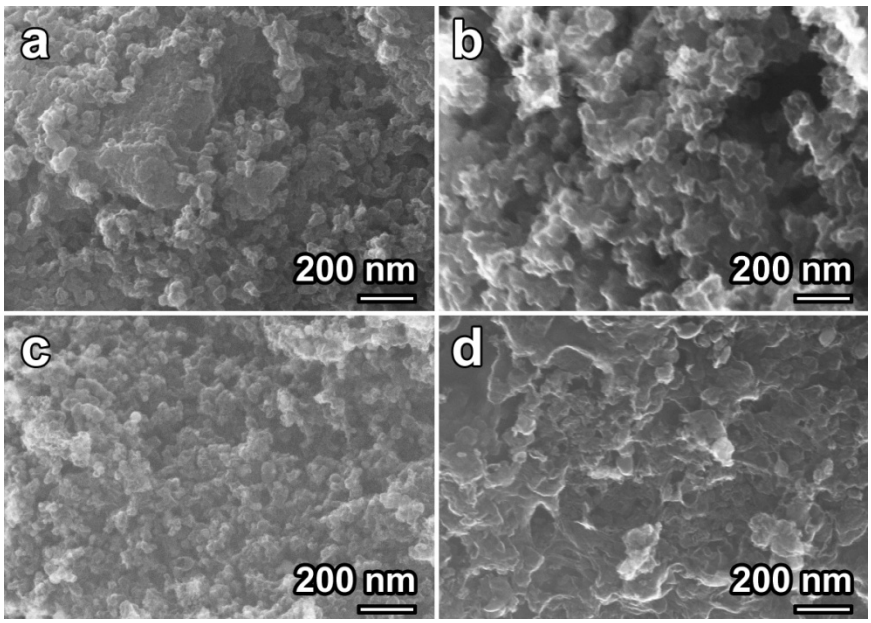

Figure 1. Scanning electron micrography images of a) functionalized KJ600, b) coated KJ600 prior to pyrolysis treatment, c) Fe-cyan-KJ600-2, and d) Fe-cyan-KJ600-3. Images were taken using a LEO FESEM at 100k times magnification at 20keV.

Three samples were synthesized and tested to determine the effect of various preparation treatments: (a) Fe-cyan-KJ600-1 with one pyrolysis using no ammonia during the pyrolysis treatment, (b) Fe-cyan-KJ600-1 with one pyrolysis treatment in ammonia, and (c) Fe-cyan-KJ600-3 with two pyrolysis treatments both with ammonia as an additional nitrogen precursor. XRD analysis, shown in Figure 2, was carried out on all three samples to determine the crystalline phases present. At *ca.* 26^{o} the graphitic C(002) face can be seen in all three catalyst samples. The relative intensity of this peak is seen to be highest in the Fe-cyan-KJ600-2 sample with one pyrolysis treatment with ammonia. This can be attributed to the greater graphitized carbon exposure brought on by the treatment with ammonia. The Fe-cyan-KJ600-3 catalyst sample was also treated with ammonia for both pyrolysis treatments which would expose greater graphitized carbon from the Ketjen Black EC-600JD surface, however, the increased loading of cyanamide and iron precursor added during second coating step may not have been effectively etched away during the second pyrolysis. This hypothesis is supported by the SEM images obtained for the Fe-cyan-KJ600-3 catalyst where there is severe agglomeration seen within the particles and increased carbon particle sizes. XRD analysis also revealed iron present in the form of iron crystals (Fe), iron carbide (Fe_7C_3) and iron nitride (Fe_3N and Fe_4N) (16) with respective peaks indicated on the diffractogram in Figure 2. Each catalyst sample was thoroughly treated with sulfuric acid to ensure surface metals on the

catalyst were removed, thus, the metal and metallic species remaining are likely to remain on the catalyst as encapsulated particles trapped under carbon layers. This result is widely supported by literature and several groups have even attempted to argue that the encapsulated iron particles facilitate the formation of ORR active sites owing to the change in electron effect near nitrogen functionalities. However, they claimed that the encapsulated iron particles themselves were not the sites for oxygen reduction (17).

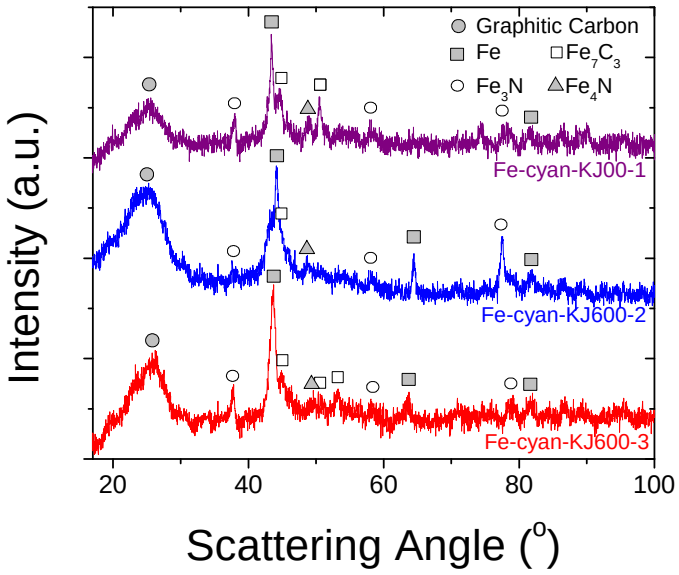

Figure 2. XRD patterns for Fe-cyan-KJ600-1, Fe-cyan-KJ600-2, and Fe-cyan-KJ600-3.

To investigate the significance of pore volume and surface area on the catalytic activity, nitrogen adsorption and desorption isotherms were measured (graphs not shown here). A summary of the resulting analysis is outlined in Table I. Each isotherm plot demonstrated characteristics indicative of micro/mesoporous carbons and pore condensation at high relative pressures. As expected, with each sequential coating and pyrolysis step, total pore volume decreases as nitrogen functionalities and carbon coatings have been impregnated into the pores. An increased pore volume was observed for the first pyrolysis using NH_3 gas compared to the first pyrolysis without NH_3. This is believed to be due to the etching and reaction of ammonia with the existing coating prior to pyrolysis. Ammonia gas facilitates the destruction of the coating and utilizes the excess nitrogen to form active site complexes on the surface of the carbon. This result is reflected in the BET surface areas calculated between the first pyrolysis samples with and without ammonia as a nitrogen precursor. There is a dramatic increase in BET surface area seen in the pyrolysis with ammonia due to the uncovering of blocked pore channels and removal of the coating into a denser active site surface. It is also important to note how this total pore volume and BET surface area changes as a second pyrolysis stage is introduced to the procedure. A drastic decrease in BET surface area is observed, even with half loading of the cyanamide and iron precursor coating. This decrease in BET surface area does not correlate with the increase in electrochemical ORR performance as seen later in this report. This discrepancy is surprising and further works need to be carried out to understand the correlation of this result to the effect on catalytic performance.

TABLE I. Summary of N_2 Adsorption/Desorption Analysis

Sample	BET Surface Area (m^2/g)	Average Pore Size (nm)	Total Pore Volume (cm^3/g)
Functionalized KJ600	1416	6.1	2.391
Fe-cyan-KJ600-1	603	3.8	0.8373
Fe-cyan-KJ600-2	1194	2.2	1.603
Fe-cyan-KJ600-3	113	1.1	0.3345

Figure 3 illustrates the ORR activity of the different catalyst samples as measured by RDE experiments at 1600rpm. It can be seen that the Fe-cyan-KJ600 catalyst without ammonia in the pyrolysis exhibits poor performance by itself as the ORR polarization curve shows a low onset and half-wave potential. For non-precious Fe-N/C catalysts it is typical to experience poorly defined plateaus in the mass limiting potential range. This is because of the relative slow kinetics compared to platinum catalysts, and an uneven active site distribution that can be brought on by the porous nature of the carbon. This result is highly supported by literature (18).

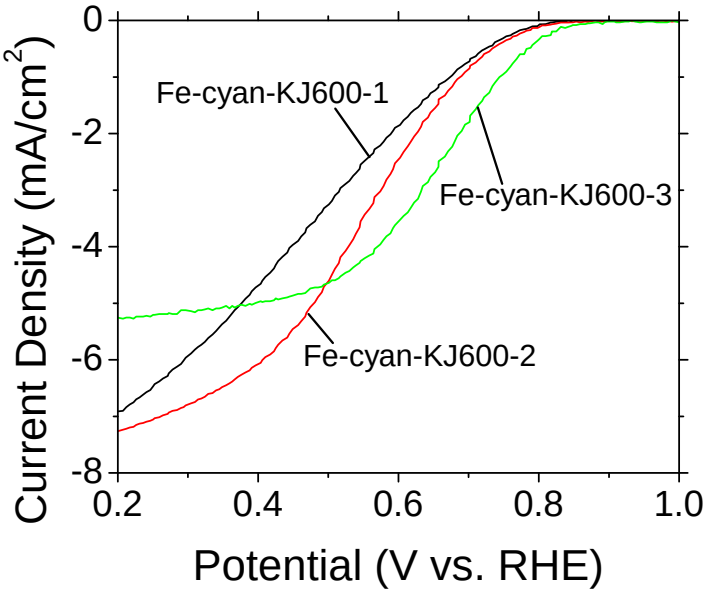

Figure 3. ORR Polarization curves of Fe-cyan-KJ600-1, Fe-cyan-KJ600-2, and Fe-cyan-KJ600-3 catalyst samples.

As hypothesized, the addition of NH_3 as a nitrogen precursor added to the pyrolysis stage significantly improved the observed half-wave potential by 0.18V. A second pyrolysis using ammonia also improved the performance of the Fe-cyan-KJ600 catalyst slightly by an additional 0.06V. A problem seen with the ORR polarization curve after a second pyrolysis is the dramatic reduction in limiting current density. Several factors were hypothesized to cause this, most significantly, the low BET surface area. It was also postulated that ball-milling of the catalyst sample cause damaging or blockage of previously synthesized active sites. During the ball-mill stage, graphitic sheets of carbon can shift to cover up active sites and reduce the overall BET surface area of the catalyst.

Conclusions

Cyanamide as a lone nitrogen precursor for these types of catalyst resulted in a poor Fe-cyan-KJ600 electrocatalyst which demonstrated low onset (0.82V vs. RHE) and half-wave (0.48V vs. RHE) potentials. Regardless of the nitrogen ratio in the organic nitrogen precursor, cyanamide by itself did not outperform other organic nitrogen precursors tested by our group previously. Successful use of ammonia gas as an additional nitrogen precursor to increase the ORR catalytic performance was carried out and resulted in higher onset and half-wave potentials of 0.83 and 0.58V vs. RHE respectively after a first pyrolysis.

A further enhancement of the ORR performance was seen after a second coating and pyrolysis (with ammonia) treatment was done. It was found that although the second coating and pyrolysis was able to increase the half-wave (0.68V vs. RHE) and onset (0.94V vs. RHE) potentials by and increasing the number of active sites, the limiting current density was diminished. This result is possibly due to the reduction of relative pyridinic nitrogen which is transformed to quaternary type nitrogen on the catalytic surface. BET analysis provided no conclusive evidence that nitrogen functionalities and active sites are hosted within the pores of the carbon support.

Acknowledgements

The University of Waterloo and the Natural Sciences and Engineering Research Council of Canada (NSERC) are gratefully acknowledged for their financial support for this work.

References

1. K. Gong, F. Du, Z. Xia, M. Durstock and L. Dai, *Science*, **323**, 760 (2009).
2. C. Bezerra, L. Zhang, K. Lee, H. Liu, J. Zhang, Z. Shi, A. Marques, E. Marques and S. Wu, *Electrochim. Acta*, **53**, 7703 (2008).
3. P. Matter, E. Wang, M. Arias, E. Biddinger and U. Ozkan, *J. Mol. Catal. A: Chem.*, **264**, 73 (2007).
4. C. Bezerra, L. Zhang, K. Lee, H. Liu, A. Marques, E. Marques, H. Wang and J. Zhang, *Electrochim. Acta*, **53**, 4937 (2008).
5. M. Lefevre, E. Proietti, F. Jaouen and J. Dodelet, *Science*, **324**, 71 (2009).
6. G. Liu, X. Li, P. Ganesan and B. Popov, *Appl. Catal., B*, **93**, 156 (2009).
7. M. Lefevre, E. Proietti, F. Jaouen and J.-P. Dodelet, *ECS Trans.*, **25**, 105 (2009).
8. J.-Y. Choi, R. S. Hsu and Z. Chen, *J. Phys. Chem. C*, **114**, 8048 (2010).
9. V. Nallathambi, J. Lee, S. Kumaraguru, G. Wu and B. Popov, *J. Power Sources*, **183**, 34 (2008).
10. G. Wu, K. Artyushkova, M. Ferrandon, J. Kropf, D. Myers and P. Zelenay, *ECS Trans.*, **25**, 1299 (2009).
11. G. Wu, Z. Chen, K. Artyushkova, F. Garzon and P. Zelenay, *ECS Trans.,* **16,** 159 (2008).
12. E. Proietti and J. Dodelet, *ECS Trans.*, **16**, 393 (2008).
13. M. Lefèvre and J. Dodelet, *Electrochim. Acta*, **53**, 8269 (2008).
14. H. T. Chung, C. M. Johnston and P. Zelenay, *ECS Trans.*, **25**, 485 (2009).

15. H. T. Chung, C. M. Johnston, F. H. Garzon and P. Zelenay, *ECS Trans.*, **16**, 385 (2008).
16. R. Yang, T. R. Dahn, H. M. Dahn and J. R. Dahn, *J. Electrochem. Soc.*, **155**, B327 (2008).
17. N. Subramanian, X. Li, V. Nallathambi, S. Kumaraguru, H. Colon-Mercado, G. Wu, J. Lee and B. Popov, *J. Power Sources*, **188**, 38 (2009).
18. H. Zhang, Q. Jiang, L. Sun, X. Yuan, Z. Shao and Z. Ma, *Int. J. of Hydrogen Energy* (2010), doi:10.1016/j.ijhydene.2009.12.015.